Epidemiology, genetic diversity and clinical manifestations of arboviral diseases in Venezuela

Lizarazo, Erley F.

DOI:
10.33612/diss.108089934

2

Spatial Dynamics of Chikungunya Virus, Venezuela, 2014

E. Lizarazo*
M.F. Vincenti-Gonzalez *
M.E. Grillet
S. Bethencourt
O. Diaz
N. Ojeda
H. Ochoa
M.A. Rangel
A. Tami

*These authors contributed equally to this work

Emerg Infect Dis. 2019;25(4):672-680.

ABSTRACT

Since chikungunya virus emerged in the Caribbean region in late 2013, around 45 countries have experienced chikungunya outbreaks. We describe and quantify the spatial and temporal events following the introduction and propagation of chikungunya into an immunological naïve population from the urban north-central region of Venezuela during 2014. The epidemic curve (n=810 cases) unraveled within five months with an R_0 = 3.7 and a radial spread traveled distance of 9.4 Km at a mean velocity of 82.9 m/day. The highest disease diffusion speed occurred during the first 90 days, while space and space-time modeling suggest that the epidemic followed a particular geographical pathway with spatio-temporal aggregation. The directionality and heterogeneity of transmission during the first introduction of chikungunya, indicated existence of areas of diffusion and elevated risk of disease occurrence and highlight the importance of epidemic preparedness. This knowledge will help manage future threats of new or emerging arboviruses.

INTRODUCTION

Chikungunya, a reemerging mosquito-borne viral infection, is responsible for one of the most explosive epidemics in the Western hemisphere in recent years. Since its introduction in the Caribbean region at the end of 2013, chikungunya virus (CHIKV) rapidly expanded within a year to most countries of South, Central and North America (*1,2*). CHIKV belongs to the genus *Alphavirus* (Togaviridae) first isolated in Tanzania during 1952 (*3*). The sylvatic (enzootic) cycle of CHIKV in Africa involves non-human primates with the virus being transmitted by an ample range of forest-dwelling *Aedes* spp. mosquitoes (*4*). Within the urban (human) cycle across Asia, the Indian Ocean and the Americas, CHIKV is transmitted by *Aedes aegypti* and *Ae. albopictus* (*5-7*). Most infected individuals (72-93%) develop symptomatic disease characterized by fever, rash and incapacitating arthralgia progressing in an important proportion of patients to chronic long-lasting relapsing or lingering rheumatic disease (*8,9*). The lack of population immunity to chikungunya in the Americas alongside the ubiquitous occurrence of competent *Ae. aegypti* and human mobility may explain the rapid expansion of CHIKV across the continent with monthly doubling of cases during the epidemic exponential phase (*10,11*). At the end of 2014, more than 1 million suspected and confirmed cases, including severe cases and deaths, were reported in 45 countries and territories while this figure reached almost 3 million cases by mid-2016 (*12*). Likely, the real number of cases is higher due to misdiagnosis with dengue and underreporting.

In Venezuela, the first official imported case was reported in June 2014 with local transmission soon following. Chikungunya quickly spread causing a large national epidemic affecting the most populated urban areas of northern Venezuela where dengue transmission is high. Given the paucity of official national data, epidemiological inference was used to estimate the number of cases. Although nationally the disease attack rate was estimated between 6.9 % and 13.8 % (*13*), the observed attack rate in populated urban areas was around 40-50% comparable to those reported in Dominican Republic (*14*), Asia and higher than those in La Reunion (*15,16*).

The rapid expansion and worldwide spread in the last decade make CHIKV one of the most public health-relevant arboviruses (*17*). With the (re)-emergence of other arboviruses, new large-scale outbreaks in the near future seem likely (*18*). Understanding and quantifying the introduction and propagation range in space and time of the initial epidemic wave of CHIKV within the complex urban settings of Latin America will shed light on arboviral transmission dynamics. This knowledge will help manage future threats of new or emerging arboviruses operating under similar epidemiological dynamics. This study characterized the epidemic wave of CHIKV in-a region highly affected by the 2014 outbreak in Venezuela. To this end, we i) described the spatial progression of the epidemic using Geographical Information Systems (GIS), ii) quantified the global geographic path that CHIKV most likely followed during the first six months of the epidemic by fitting a polynomial regression model (trend surface analysis), iii) determined the general direction and speed of the propagation wave of the disease, and finally iv) identified the local spatial-time disease clusters through spatial statistics.

MATERIALS AND METHODS

STUDY AREA:

Carabobo State, is situated in the north-central region of Venezuela (Figure 1) and is one of the most densely populated regions (19).

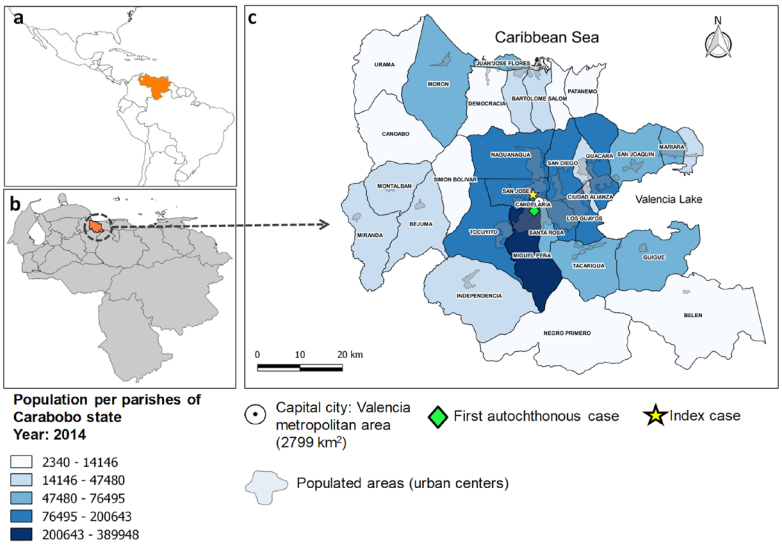

Figure 1. Area of study on the spatial dynamics of chikungunya virus, Venezuela, 2014. A) Venezuela. B) Carabobo State (2014 population: 2,415,506 inhabitants). C) Parishes of Carabobo State. The grading of color blue depicts the population per parish up to 2014. Most persons live in the capital city of Valencia (892,530 inhabitants); within the metropolitan area, poorer settlements are located mainly in the southern area, and the most organized and urbanized medium- and high-level neighborhoods are situated toward the north-central part.

STUDY DESIGN AND DATA COLLECTION:

A retrospective study of patient and epidemiological data collected through the national Notifiable Diseases Surveillance System (NDSS) was performed to understand the spatio-temporal spread of the 2014 chikungunya epidemic at a local and global scale. A total of 810 patients of all ages were diagnosed as suspected chikungunya-infected cases by their physicians and were reported via the NDSS to the epidemiological department of the Regional Ministry of Health (INSALUD) of Carabobo State. Patients suspected of chikungunya were those presenting with fever of sudden appearance, rash and joint pain with or without other flu-like symptoms. Patients who attended public or private health care centers across Carabobo State municipalities were included in this study. Patient data was obtained for the period between June 10th and December 3rd 2014 (epidemiological weeks [EW] 22-49) coinciding with the Venezuelan chikungunya outbreak. Data corresponding to the first visit of the patients to a healthcare center was included and comprised patient address, clinical manifestations and epidemiological risk factors. The information was entered in a database, checked for consistency and analyzed anonymously. The index case (IC) was defined as the first chikungunya patient reported by the NDSS within this region.

TEMPORAL DYNAMICS OF CHIKUNGUNYA SPREAD

We described the growth rate of the disease by plotting the cumulative cases per EW and fitted a logistic curve after examining the shape of the epidemiological curve (Figure A1). The average number of secondary cases resulting from a primary case in a completely susceptible population, e.i. the epidemic's basic reproductive number (R_0), was derived as follows: We estimated R0 from the initial phase of the epidemic using the exponential growth method (20) and then calculated a real-time estimate of R_0, called Rt (21,22) to explore the time-varying transmissibility of chikungunya (Technical Appendix).

SPATIO-TEMPORAL TREND OF THE EPIDEMIC WAVE OF CHIKUNGUNYA

The address of every patient was georeferenced into a GIS so that the Xi (east-west) and Yi (north-south) coordinates of each chikungunya case were derived. We drew the weekly spatial progression of the 810 reported chikungunya cases with respect to the IC in a map. To assess the spreading pattern before the epidemic reached the steady (plateau) state (Figure 2), we selected cases between 0-125 days (EW-40) after the IC appearance. Within this time range the case notification rate maintained a sustained growth.

To explore the general spatial trend of chikungunya cases (or the movement of the epidemic wave of infection) across the study area, a map of time of disease spread was developed using Trend Surface Analysis (TSA), a global surface fitting methodology (explanation found in Technical Appendix). The variable time (in days) was created using the symptoms onset date from the IC as the baseline date across the 810 case localities, i.e. time (Xi, Yi). Thus, time is considered as the number of days elapsed between the appearance of a case in a specific locality Zi and the IC. Results of the TSA were used to generate a contour map or smoothed surface, with each contour line representing a specific predicted time-period in this urban landscape setting since the initial invasion of the virus. The local rate and direction of the spread of infection was estimated as the directional derivative at each case using the TSA fitted model to obtain local vectors that depicted the direction and speed (inverse of the slope along the direction of the movement) of infection propagation from each locality in X and Y directions. Additionally, we used kriging, a local geostatistical interpolation method, to generate an estimated continuous surface from the scattered set of points (i.e. time) with z-value to better capture the local spatial variation of chikungunya spread across the urban landscape (23). We used 'ordinary kriging' to predict values of the time-period since the initial invasion of the virus. We selected the model with the best fit out of three theoretical variogram models tested by cross-validation to predict the values at unmeasured locations and their associated errors (Technical Appendix).

We also obtained an empirical basic baseline rate of disease spread to quantify the observed velocity for each case zi directly from the data by measuring the linear distance (meters) of case Zi to the IC and then dividing it by the time in days that elapsed since the IC was reported. Differences between velocities were assessed using Kruskal-Wallis test, a non-parametric method to test differences between groups when these are non-normally distributed (24).

Finally, to identify: a) general space-time clusters of chikungunya transmission we performed a Knox analysis (25) and b) interactions at specific temporal intervals using the incremental Knox test (IKT) (26) For (a) we selected critical values of 100 meters (distance) and three weeks

(time) after multiple distance and time windows testing (Table A2). Our selection was based on *Aedes* mosquito flight range and the maximum duration of the intrinsic and extrinsic incubation periods of the virus, respectively (27,28). Upon identification of the cluster, the distance between the first case of a cluster (C1) and the cases within the cluster Zi was calculated, considering this distance as a measure of virus disease spread. For (b) the IKT was used in an exploratory mode over the time intervals from 1 to 31 days, and space distances from 25 to 500 m (Technical Appendix). Spatial analyses were carried out with R software (The R-Development Core Team, http://www.r-project.org) and ArcGIS (v.10.3, ESRI Corporation, Redlands, CA) using the Spatial Analyst Toolbox, whilst maps were generated with Quantum GIS 2.14.3 Essen (GNU—General Public License) software. Space-time (Knox) analysis was performed using ClusterSeer 2.0 (Terraseer, Ann Arbor, MI).

ETHICS STATEMENT

Data were analyzed anonymously and individuals were coded along with the information of address with a unique numeric identifier. The study was approved by the epidemiological department of the Regional Ministry of Health (INSALUD) of Carabobo State.

RESULTS

TEMPORAL DYNAMICS OF CHIKUNGUNYA SPREAD

A total of 810 suspected chikungunya cases were reported in Carabobo State in 2014 during epidemiologic weeks 22–49 (28 weeks) representing the first introduction and propagation of the virus in the north-central region of Venezuela. The index case was an imported case (in a returning traveler from the Dominican Republic) in epidemiologic week 22 in the north-central zone of the capital city (Valencia) (Figure 1). The index case was followed by the other imported cases and soon after by locally transmitted cases.

The cumulative cases during epidemiologic weeks 22–49 followed a logistic growth (Appendix Figure 1; R = 0.99, n = 810, $p<0.05$). The reported cases displayed a characteristic epidemic curve with a single wave and peaked at epidemiologic week 33, eleven weeks after the index case (Figure 2). The epidemic takeoff occurred at epidemiologic week 31, i.e., 9 weeks after the index case. The total duration of the outbreak was ~28 weeks; however, the main epidemic curve lasted from epidemiologic week 30 until epidemiologic weeks 43–44, ~3 months. The initial global growth rate of the epidemic was 0.53 cases per week, and R_0 = 3.7 (95% CI 2.78–4.99) secondary chikungunya cases per primary case (epidemiologic weeks 22–31). We obtained comparable results when we calculated the instantaneous reproductive number (R_t = 4.5, 95% CI 2.4–7.1) during the epidemic peak. From epidemiologic week 34, R_t values fell below 1 and gradually decreased from there onward (Appendix Figure 2).

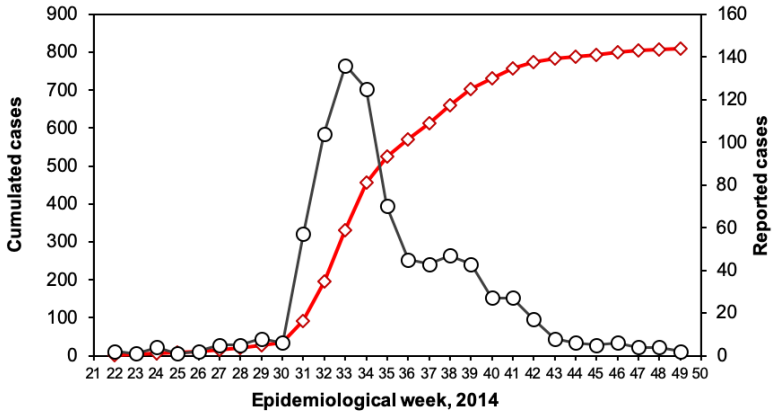

Figure 2. Reported chikungunya cases during the epidemic, Carabobo State, Venezuela, 2014. Black line with open black dots, chikungunya cases; red line with open red diamonds, cumulative cases.

SPATIOTEMPORAL DISTRIBUTION OF THE CHIKUNGUNYA EPIDEMIC

The chikungunya outbreak progressed chronologically and spatially through Carabobo State (Figure 3; Video, https://wwwnc.cdc.gov/EID/article/25/4/17-2121-V1.htm). The cases reported in Valencia during the first 6 weeks were located in the central area of the city close to the index case, whereas a few cases were reported in the southwestern part of Valencia and in other small urban towns of Carabobo (Figure 3, panel A). The first autochthonous case occurred during this interval in the south-central area of Valencia, relatively close to the index case (Figure 3, panel A). During epidemiologic weeks 28–31, the number of reported cases increased in parishes around the autochthonous case (Figure 3, panel B). During epidemiologic weeks 32–35, the number of cases exploded exponentially, and the disease spread rapidly throughout the capital city and surrounding smaller urban centers (Figure 3, panel C). New cases were actively reported during 8 continuous weeks (Figure 3, panels C, D) to later decrease from epidemiologic week 40 to epidemiologic week 49 (Figure 3, panels E, F). The epidemic progressed in two directions (movement axes) in the region: a north–south direction and a northeastern and southwestern direction. Both shifts consistently overlapped with the populated centers of the region and the main traffic routes (motorways and main roads).

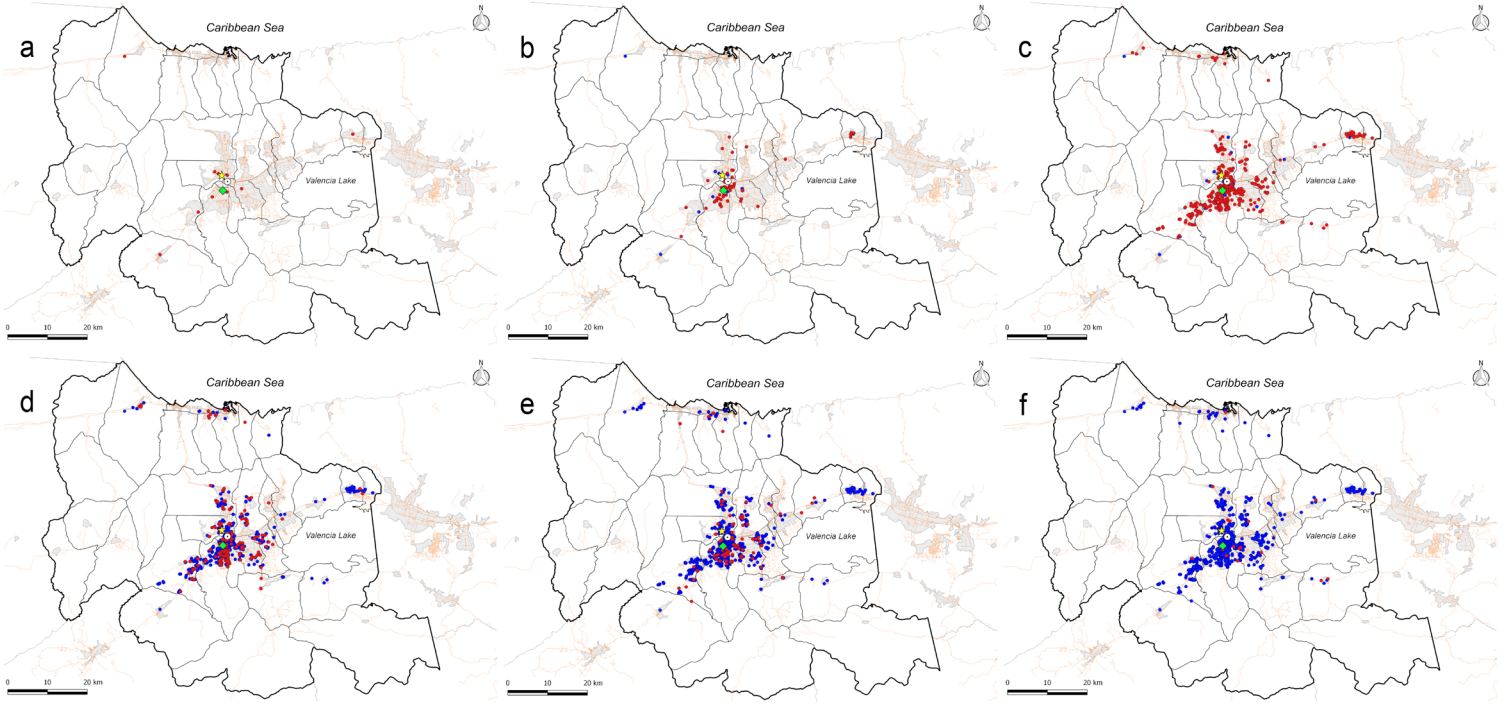

Figure 3. Spatial and temporal spread of the chikungunya epidemic, Carabobo State, Venezuela, June–December 2014. Time is presented at EW intervals as follows: A) EW 22–27. B) EW 28–31. C) EW 32–35. D) EW 36–39. E) EW 40–45. F) EW 46–49. Red circles indicate the appearance of new cases for the given interval; blue indicates the cumulative cases in prior intervals. Light yellow lines depict the road system of the area of study; light gray areas represent the populated areas (urban centers) within the parishes. Yellow star indicates index case; green diamond indicates first autochthonous case. EW, epidemiologic week.

Figure 4, panel A depicts the general direction and propagating wave of disease derived from the Trend Surface Analysis. Contour lines that are far apart indicate that the epidemic diffused quickly through the area whereas lines that are closer show a slower progression. The direction of diffusion is also given by the edges of the contour lines. The model located the wave of disease dispersal in the central part of the region and included the index case and autochthonous case. The bulk of the outbreak unfolded within 90 days, spreading mainly to the southwestern and northern parts of the capital city. During this time, the maximum radial distance traveled was 9.4 km. A slower diffusion was predicted toward the northeast and southern part of the region. However, the limitation of the method resulting from edge effects determines that the best area for prediction is the central one.

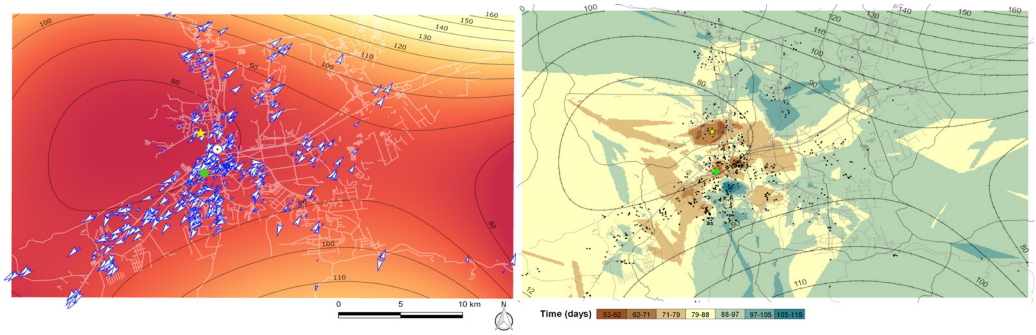

Figure 4. Global and local predicted spreading patterns of chikungunya virus, Carabobo State, Venezuela, 2014. A) Contour map (global scale) of the predicted spreading waves and the velocity vector arrows of each case of chikungunya. The contour map and contour lines in black (traveling waves) were estimated by the best-fit trend-surface analysis (3rd order polynomial model) of time (days) to the first reported case or index case of chikungunya across the landscape. White lines correspond to the road system of the area. The background gradient of color shows the probability of chikungunya virus diffusion according to the prediction of the model: the darker the red, the higher the probability of spread. Each vector (blue outlined arrows) represents the instantaneous velocity derived from the partial, differential equations from the Trend Surface Analysis model (Appendix). B) Spatial prediction map for the ordinary kriging (Gaussian model) interpolation of the time (each color represents different days) of chikungunya spread. Contour lines from Trend Surface Analysis depicted in the kriging surface are shown only for comparison purposes. Yellow star indicates index case; green diamond indicates first autochthonous case.

To visualize the local diffusion of CHIKV at each location, we drew the vector field across the modeled surface (Figure 4, panel A). Overall, the model confirms the previous observation of a general trend or corridor of diffusion of chikungunya cases southwest and northeast of the capital city within the first 80 days. After 90 days, the epidemic wave varied its direction and magnitude by location. Although agreeing with the general pattern shown by the Trend Surface Analysis, the resulting kriging Gaussian (selected) model interpolation surface (Figure 4, panel B; Appendix Table 1) predicts a more heterogeneous spread pattern of chikungunya cases by matching the patchy (uneven population density) distribution of human neighborhoods and the road network. In addition, kriging identified: 1) a faster propagation of the epidemiologic wave at the southwestern and eastern areas where the model showed its best fit (Appendix Figure 3, panel A) and 2) a slower movement to the northeastern and south-central areas than estimated by the Trend Surface Analysis.

We calculated the virus diffusion velocities for each parish through the empirical method (Table 1). The mean velocity of disease spread across the state was 82.9 m ± 53.6 m/day, and overall, the pattern of diffusion of CHIKV was highest in the suburban and rural settlements near the capital city. However, the observed velocities varied significantly by location ($p<0.05$, n = 735). For instance, the parishes at the center of the capital (San Jose, Catedral, Candelaria, San Blas, Santa Rosa) showed velocities <60 m/day, whereas in the remaining localities, including both rural and suburban towns, the speed was >60 m/day. The maximum velocity of the outbreak was of 483 m/day measured south of the capital.

Table 1. Average velocities of chikungunya virus spread across Carabobo State, Venezuela, 2014

		Velocity, m/day					
Parish	No. cases	Mean	SD	95% CI	Minimum	Maximum	Location‡
Candelaria	29	39.4	15.3	33.5–45.2	17	96	Central
Catedral	11	28.8	9.5	22.4–35.3	15	50	Central
Ciudad Alianza	1	146.7	.	-	147	147	East-southeast
El Socorro	6	47.2	32.1	13.5–80.9	25	98	South-southwest
Guacara*	4	206.2	151.7	35.1–447.6	98	430	East-northeast
Guigue†	5	256.7	84.6	151.7–361.8	163	344	Southeast
Independencia*	6	206.7	64.7	138.8–274.5	138	310	South-southwest
Los Guayos	42	115.1	31.4	105.3–124.9	52	176	East-southeast
Miguel Peña	228	80.6	40.6	75.3–86.0	21	483	South
Naguanagua	41	85.9	27.3	77.3–94.6	47	174	North
Rafael Urdaneta	84	87.2	35.3	79.5–94.8	23	186	Southeast
San Blas	27	43.6	11.7	39.0–48.3	21	62	Central
San Diego	35	73.3	28.5	63.5–83.1	41	150	North-northeast
San Jose	68	27.6	26.2	21.3–34.0	0	202	North-central
Santa Rosa	70	58.4	10.4	55.9–60.9	35	97	Central
Tacarigua†	6	197.0	47.0	147.7–246.3	149	259	South-southeast
Tocuyito*	70	149.8	52.8	137.2–162.4	61	365	Southwest
Yagua†	2	111.0	12.7	3.4–225.4	102	120	East-northeast
Carabobo	735	82.9	53.6	79.0–86.7	0	483	-

*Dormitory urban settlements.
†Rural settlements.
‡Location refers to relative locations from the center of the capital city, Valencia.

SPATIOTEMPORAL CLUSTERS OF THE EPIDEMIC WAVE

Results after multiple space and time parameters testing showed that core clusters remained similar through time (Appendix Figure 4), and the relative risk (RR) within the clusters remained important (RR>1.5) up to 3 weeks (Appendix Figure 5). Using selected critical values, we identified 75 general space–time clusters using Knox analysis (Appendix Table 3; Appendix Figure 6, panel A). These clusters included at least 2 space–time-linked cases and a total of 205 (27.9%) cases that showed a space–time relation. The major accumulation of clusters occurred in the southern and southwestern part of the capital. The earliest cluster (cluster 7, Figure 5) was located in the west-central part of the capital and comprised 3 cases, including the index case. From this cluster, the average distance from each case to the index case was 32 m, and the cases were reported within 25 days after the index case. In addition, the major cluster (cluster 57, 12 cases) was located in the west-central area of the capital 4 km from the index case (Figure 5). The cases belonging to this cluster occurred within 9 days (1.3 cases per day); these cases occurred an average of 70 days (range 69–77 days) after the index case (Appendix Table 3). The median time between the first notified case (symptom onset) and the last case within a cluster was 9 days (range 3–18 days). Furthermore, the average distance between cases within

the clusters was 75.2 m ± 25.6 m (range 110.6 m–39.2 m) (Appendix Table 4). Furthermore, the baseline velocity in Carabobo State was similar to the average velocity within the clusters (69.9 ± 34.4 m/day). These results agree with IKT findings, where the temporal intervals with the strongest spatial clustering and RR occurred 1–7 days and 25–150 m (Appendix Figures 7, 8).

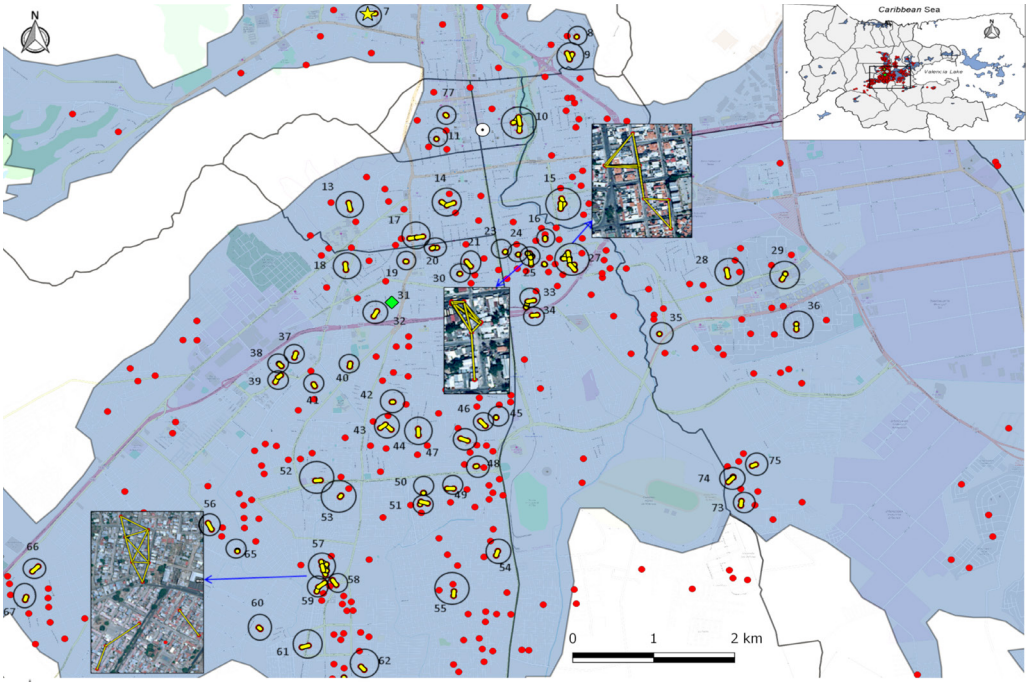

Figure 5. Geographic distribution and significant space–time clustering of reported chikungunya cases identified in a section of the capital city, Valencia (metropolitan area), Carabobo State, Venezuela, June–December 2014. Upper right corner depicts Carabobo state geographic location, the black rectangle on it shows the area zoomed in to better detail of the clusters. Red dots denote case location; black outlined circles identify a significant space–time cluster; yellow lines show the interaction between cases (time–space link). The analysis was performed using 100 m as clustering distance and 3 weeks as time window. Significance level for local clustering detection was $p<0.05$.

DISCUSSION

We described and quantified the spatial and temporal events that followed the introduction and explosive propagation of CHIKV into an immunologically naïve population living in the urban north-central region of Venezuela during 2014. The main epidemic curve developed within 5 months, with a maximum value of the estimate of R_0 = 3.7 by epidemiologic week 12. The speed of disease diffusion was greatest during the first 90 days, and the spatial spread was heterogeneous following mostly a southwest spatial corridor at a variable local rate of diffusion across the landscape. The radial spread traveled distance was 9.4 km at a mean velocity of 82.9 m/day. The chikungunya epidemic showed spatiotemporal aggregation predominantly south of the capital city, where conditions for human–vector contact are favorable.

The temporal dynamics here described, R_0 and its time variable form $R_{t,}$ suggest high transmissibility of CHIKV in this population. These results agree with previous CHIKV

introductions into naïve populations (*29*–*31*) and with the 2014 predicted values for mid-latitude countries (R_0 = 4–7) of the Americas (*31*). High values of R_0 are also described during first introduction outbreaks of other *Aedes*-borne infections, such as dengue in Chile (R_0 = 27.2) (*32*) and Zika virus in Brazil (R_0 = 1.5–6); (*33*) and French Polynesia (*34*). Yet, overall R_0 estimates for dengue are ~2–6 (*35*). The similarity between the R_0 of chikungunya, dengue, and Zika virus infection, all transmitted by the same main vector, *Ae. aegypti,* strongly suggests that the major factor driving the exponential increase of the epidemic curve of arboviruses in naïve populations, is the transmission efficiency of the vector.

Spatially, Trend Surface Analysis and kriging analysis showed a primary wave of disease spread within the first 80 days in the most likely area of transmission (the southwestern center of Valencia), whereas a second wave at 90 days showed the spread of cases toward the southern, western, and northern areas. This sequential pattern is similar to that of dengue, where transmission within neighborhoods most likely is driven by mosquito presence or abundance and/or short-distance movement of viremic hosts (*36*–*38*), whereas long-distance dissemination is probably generated by human mobility patterns through main roads and motorways. Both movements powerfully affected disease transmission (*39,40*). Moreover, population density modulates the chance of vector–host contact (*30,41*). This is reflected in the variation of calculated velocities across different spatial points and the increased diffusion speed of the epidemic toward the southernmost populated area.

Although CHIKV was introduced into a naïve population, the distribution of cases was not random but aggregated into 75 significant space–time clusters, indicating an increased likelihood of vector–host contact. The area with most clusters, the southern part of Valencia city, is characterized by densely populated neighborhoods, lower socioeconomic status, and crowded living conditions. Similar factors increased the risk for dengue transmission and clustering (hot spots) in highly endemic urban areas of Venezuela (*42*). Poverty and human behavior fostering potential mosquito breeding sites (such as storing water at home) were linked with a greater risk for dengue (*42,43*). In Venezuela, long-lasting deficits in public services, such as frequent and prolonged interruptions in water supply and electricity, have become regular in recent years. These inadequacies have obliged residents to store water, maintaining adequate breeding conditions for *Aedes* vectors during the dry season and throughout the year (*44*). During the CHIKV epidemic, the proportion of houses infested with *Aedes* larvae/pupae (house index) in Venezuela was >20% (*45*). The World Health Organization recommends a house index <5% for adequate vector control (*46*).

In our study, the average distance among cases within chikungunya clusters was 75 m, which coincided with the reported flying range of urban *Ae. aegypti* females during mark-release-recapture studies (*37,47*). *Ae. aegypti* females have been reported to visit a maximum of 3 houses in a lifetime while not traveling far from their breeding sites (*48,49*). Thus, the distance traveled by the vector and the number of possible host encounters with an infected vector cannot explain the entire disease epidemic spread. Other factors, such as movement of viremic hosts, a widely distributed vector, and the lack of herd immunity may play a role, as for dengue, in long-range spread (*37*).

The lack of entomologic data and estimates of human movement limit our study. We expect that our estimates based on epidemiologic records are accurate because chikungunya is symptomatic

in >80% of cases. Likewise, surveillance in Venezuela is based on symptomatic patient reporting by treating doctors.

Our analysis suggests that the epidemic of chikungunya followed a determined geographic course. This propagation was potentiated south and southwest of the study area. Chikungunya is now established in Venezuela, along with other *Aedes*-borne infections, such as dengue and Zika virus infection. However, further epidemics of these and other reemergent arboviruses, i.e., Mayaro virus (*18,50*), are likely to arise. The insights gained in our study will help understand and predict future epidemic waves of upcoming vectorborne infections and to quickly define intervention areas and improve outbreak preparedness response in Venezuela and countries with similar settings.

ACKNOWLEDGMENTS

We thank Carenne Ludeña for the support and valuable insights regarding the analysis in this research. We thank Jared Aldstadt who kindly shared the R code for the IKT analysis.

This work was supported by the Department of Medical Microbiology, University Medical Center Groningen (UMCG), University of Groningen, Groningen, the Netherlands. E.L. and M.V.-G. received the Abel Tasman Talent Program grant from the UMCG, University of Groningen, Groningen, the Netherlands. M.E.G. received a Travel Grant from The Netherlands Organization for Scientific Research (grant no. 040.11.590/2129), the Netherlands, 2017.

ABOUT THE AUTHOR

Mr. Lizarazo is a PhD candidate at the University Medical Center Groningen. His research interests are vector borne diseases and molecular epidemiology. Ms. Vincenti-Gonzalez is a Postdoc at the University Medical Center Groningen, her research interests are vector-borne diseases and spatial-temporal dynamics of infectious diseases.

REFERENCES

1. Weaver SC, Forrester NL. Chikungunya: evolutionary history and recent epidemic spread. Antiviral Res. 2015;120: 32–9.
2. Patterson J, Sammon M, Garg M. M. Dengue, Zika and chikungunya: emerging arboviruses in the New World. West J Emerg Med. 2016;17:671–9
3. Robinson MC. An epidemic of virus disease in Southern Province, Tanganyika Territory, in 1952-53. I. Clinical features. Trans R Soc Trop Med Hyg. 1955;49:28–32.
4. Powers AM, Logue CH. Changing patterns of chikungunya virus: re-emergence of a zoonotic arbovirus. J Gen Virol. 2007;88:2363–77.
5. Wolfe ND, Kilbourn AM, Karesh WB, Rahman HA, Bosi EJ, Cropp BC, *et al*. Sylvatic transmission of arboviruses among Bornean orangutans. Am J Trop Med Hyg. 2001;64:310–6.
6. Chevillon C, Briant L, Renaud F, Devaux C. The chikungunya threat: an ecological and evolutionary perspective.Trends Microbiol. 2008;16:80–8.
7. Higgs S, Vanlandingham D. Chikungunya virus and its mosquito vectors. Vector Borne Zoonotic Dis. 2015;15:231–40.
8. Marimoutou C, Ferraro J, Javelle E, Deparis X, Simon F. Chikungunya infection: self-reported rheumatic morbidity and impaired quality of life persist 6 years later. Clin Microbiol Infect. 2015;21:688–93.
9. Elsinga J, Gerstenbluth I, van der Ploeg S, Halabi Y, Lourents NT, Burgerhof JG, *et al*. Long-term chikungunya sequelae in Curaçao: burden, determinants, and a novel classification tool. J Infect Dis. 2017;216:573–81.
10. Zeller H, Van Bortel W, Sudre B. Chikungunya: its history in Africa and Asia and its spread to new regions in 2013–2014. J Infect Dis. 2016;214 (suppl 5):S436–40.
11. Pan American Health Organization. Number of reported cases of chikungunya fever in the Americas—cumulative cases (October 23, 2015) [cited 2017 Aug 20]. http://www.paho.org/hq/index.php?option=com_topics&view=readall&cid=5927&Itemid=40931&lang=en
12. Pan American Health Organization. Number of reported cases of chikungunya fever in the Americas- cumulative cases (October 23, 2015) [cited 2017 Aug 20]. http://www.paho.org/hq/index.php?option=com_topics&view=readall&cid=5927&Itemid=40931&lang=en
13. Oletta JF. Epidemia de fiebre chikungunya en Venezuela, 2014–2015. Gaceta Medica Caracas. 2016;124: 122–37.
14. Pimentel R, Skewes-Ramm R, Moya J. Chikungunya in the Dominican Republic: lessons learned in the first six months [in Spanish]. Rev Panam Salud Publica. 2014;36:336–41.
15. Gérardin P, Guernier V, Perrau J, Fianu A, Le Roux K, Grivard P, *et al*. Estimating chikungunya prevalence in La Réunion Island outbreak by serosurveys: two methods for two critical times of the epidemic. BMC Infect Dis. 2008;8:99.
16. Schwartz O, Albert ML. Biology and pathogenesis of chikungunya virus. Nat Rev Microbiol. 2010;8:491–500.
17. Weaver SC. Arrival of chikungunya virus in the new world: prospects for spread and impact on public health. PLoS Negl Trop Dis. 2014;8:e2921.
18. Hotez PJ, Murray KO. Dengue, West Nile virus, chikungunya, Zika-and now Mayaro? PLoS Negl Trop Dis. 2017;11:e0005462.
19. Instituto Nacional de Estadística. [cited 2017 Nov 18]. http://www.ine.gov.ve/
20.Wallinga J, Lipsitch M. How generation intervals shape the relationship between growth rates and reproductive numbers. Proc Biol Sci. 2007;274:599–604.
21. Nishiura H, Chowell G, Heesterbeek H, Wallinga J. The ideal reporting interval for an epidemic to objectively interpret the epidemiological time course. J R Soc Interface. 2010;7:297–307.
22. Coelho FC, de Carvalho LM. Estimating the attack ratio of dengue epidemics under time-varying force of infection using aggregated notification data. Sci Rep. 2015;5:18455.
23. Dale M, Fortin M. Spatial analysis: a guide for ecologists. 2nd ed. Cambridge (UK): Cambridge University Press; 2014.
24. Wallis K. Use of ranks in one-criterion variance analysis. J Am Stat Assoc. 1952;47:583–621.
25. Knox EG. The detection of space–time interactions. Journal of the Royal Statistical Society. Series C, Applied Statistics. 1964;13(1):25–29.
26. Aldstadt J. An incremental Knox test for the determination of the serial interval between successive cases of an infectious disease. Stochastic Environmental Research and Risk Assessment. 2007;21:487–500.

27. Chan M, Johansson MA. The incubation periods of dengue viruses. PLoS One. 2012;7: e50972.
28. David MR, Lourenço-de-Oliveira R, Freitas RM. Container productivity, daily survival rates and dispersal of *Aedes aegypti* mosquitoes in a high income dengue epidemic neighbourhood of Rio de Janeiro: presumed influence of differential urban structure on mosquito biology. Mem Inst Oswaldo Cruz. 2009;104:927–32.
29. Boëlle P-Y, Thomas G, Vergu E, Renault P, Valleron A-J, Flahault A. Investigating transmission in a two-wave epidemic of chikungunya fever, Réunion Island. Vector Borne Zoonotic Dis. 2008;8:207–17.
30. Yakob L, Clements ACA. A mathematical model of chikungunya dynamics and control: the major epidemic on Réunion Island. PLoS One. 2013;8: e57448.
31. Perkins TA, Metcalf CJ, Grenfell BT, Tatem AJ. Estimating drivers of autochthonous transmission of chikungunya virus in its invasion of the americas. PLoS Curr. 2015;7:7.
32. Chowell G, Fuentes R, Olea A, Aguilera X, Nesse H, Hyman JM. The basic reproduction number R0 and effectiveness of reactive interventions during dengue epidemics: the 2002 dengue outbreak in Easter Island, Chile. Math Biosci Eng. 2013;10:1455–74.
33. Ferguson NM, Cucunubá ZM, Dorigatti I, Nedjati-Gilani GL, Donnelly CA, Basáñez M-G, *et al*. EPIDEMIOLOGY. Countering the Zika epidemic in Latin America. Science. 2016;353:353–4.
34. Nishiura H, Kinoshita R, Mizumoto K, Yasuda Y, Nah K. Transmission potential of Zika virus infection in the South Pacific. Int J Infect Dis. 2016;45:95–7.
35. Johansson MA, Hombach J, Cummings DAT. Models of the impact of dengue vaccines: a review of current research and potential approaches. Vaccine. 2011;29:5860–8.
36. Waterman SH, Novak RJ, Sather GE, Bailey RE, Rios I, Gubler DJ. Dengue transmission in two Puerto Rican communities in 1982. Am J Trop Med Hyg. 1985;34:625–32.
37. Vazquez-Prokopec GM, Kitron U, Montgomery B, Horne P, Ritchie SA. Quantifying the spatial dimension of dengue virus epidemic spread within a tropical urban environment.PLoS Negl Trop Dis. 2010;4:e920.
38. Stoddard ST, Forshey BM, Morrison AC, Paz-Soldan VA, Vazquez-Prokopec GM, Astete H, *et al*. House-to-house human movement drives dengue virus transmission. Proc Natl Acad Sci U S A. 2013;110:994–9.
39. Mondini A, de Moraes Bronzoni RV, Nunes SHP, Chiaravalloti Neto F, Massad E, Alonso WJ, *et al*. Spatio-temporal tracking and phylodynamics of an urban dengue 3 outbreak in São Paulo, Brazil. PLoS Negl Trop Dis. 2009;3:e448
40. Tauil PL. Urbanization and dengue ecology] [in Portuguese]. Cad Saude Publica. 2001;17(Suppl):99–102.
41. Gubler DJ. Dengue, urbanization and globalization: the unholy trinity of the 21st century. Trop Med Health. 2011;39(Suppl):3–11.
42. Vincenti-Gonzalez MF, Grillet ME, Velasco-Salas ZI, Lizarazo EF, Amarista MA, Sierra GM, *et al*. Spatial analysis of dengue seroprevalence and modeling of transmission risk factors in a dengue hyperendemic city of Venezuela. PLoS Negl Trop Dis. 2017;11:e0005317.
43. Agha SB, Tchouassi DP, Bastos ADS, Sang R. Assessment of risk of dengue and yellow fever virus transmission in three major Kenyan cities based on Stegomyia indices. PLoS Negl Trop Dis. 2017;11:e0005858.
44. Barrera R, Avila J, González-Téllez S. Unreliable supply of potable water and elevated Aedes aegypti larval indices: a causal relationship? J Am Mosq Control Assoc. 1993;9:189–95.
45. Grillet ME, Del Ventura F. Transmisión del virus Zika: Patrones y mecanismos eco-epidemiológicos de una arbovirosis. Tribuna del Investigador. 2016;17: 42–61.
46. World Health Organization. Guidelines for dengue surveillance and mosquito control. WHO regional publication, Western Pacific Education in Action Series, no. 8. Geneva: The Organzation; 1995.
47. Harrington LC, Scott TW, Lerdthusnee K, Coleman RC, Costero A, Clark GG, *et al*. Dispersal of the dengue vector Aedes aegypti within and between rural communities. Am J Trop Med Hyg. 2005;72:209–20.
48. Rodhain F, Rosen L. Mosquito vectors and dengue virus-vector relationships. In: Gubler D, Kuno G, editors. dengue and dengue haemorrhagic fever. 1st ed. London (UK): CAB International; 1997.45-60.
49. Getis A, Morrison AC, Gray K, Scott TW. Characteristics of the spatial pattern of the dengue vector, Aedes aegypti, in Iquitos, Peru. Am J Trop Med Hyg. 2003;69:494–505.
50. Auguste AJ, Liria J, Forrester NL, Giambalvo D, Moncada M, Long KC, *et al*. Evolutionary and ecological characterization of Mayaro virus strains Isolated during an outbreak, Venezuela, 2010. Emerg Infect Dis. 2015;21:1742–50.

Video. Spatial progression of the chikungunya outbreak, Carabobo state, Venezuela, 2014. Available at https://drive.google.com/a/rug.nl/file/d/18nwM9PXwHp4M6BNYv7SVVohpH7eLtrzy/view?usp=sharing

APPENDIX

SPATIAL DYNAMICS OF CHIKUNGUNYA VIRUS, VENEZUELA, 2014

1. MATERIALS AND METHODS

1.1. ESTIMATING THE REPRODUCTIVE NUMBER (R_0)

For new emerging infectious diseases, the value of the reproductive number R_0 can be inferred indirectly from the initial epidemic phase by estimating the exponential epidemic growth rate (*r*) of new observed infections and relating these parameters to the generation time of infection (*Tg*) through the following equation (*1*).

$$R = \frac{1}{M(-r)}$$

where *M* is the moment generating function of the disease generation time distribution. A generation time distribution for chikungunya (CHIK) was defined using a gamma distribution with a mean of 1.86 weeks and a standard deviation of 0.05 weeks. This includes both the human and vector infection cycle, by assuming a short mosquito infection lifespan case as reported before by Boëlle *et al*. (*2*). For this method we applied the 'R_0' package version 1.2–6 developed by Boëlle and Obadia (*3*) (The R-Development Core Team, http://www.r-project.org).

1.2. ESTIMATING THE EFFECTIVE REPRODUCTIVE NUMBER (RT)

Given that the behavior of the force of chikungunya virus (CHIKV) infection through time was unknown, we calculated a real-time estimate of the basic reproductive number of the disease, that is the effective reproductive number at time *t* (Rt) as originally proposed by Nishiura *et al*. (*4*). We then explored the time-varying transmissibility using the Rt series derived following the methodology of Coelho and Carvalho (*5*). Hence, Rt was estimated as

$$Rt = \left(\frac{Y_{t+1}}{Y_t}\right)^{1/n}$$

where Y_t and Y_{t+1} are taken to be the number of reported disease cases for a particular time *t* and *t+1*, respectively, while *n* defines the ratio between the length of the reporting interval and the mean generation time of the disease. The reporting interval was defined as the duration of an epidemiologic week (7 days), while the generation time was assumed to be of 2 weeks as established above. To run the calculation, we applied the R code developed by Coelho and Carvalho (*5*) available on the GitHub repository at https://github.com/fccoelho/paperLM1 (The R-Development Core Team).

1.3. TREND SURFACE ANALYSIS (TSA) AND LOCAL VECTORS OF DIRECTION AND SPEED OF INFECTION

TSA methodology consists in fitting, through the method of least squares, a function in a multiple-regression–like procedure where the response variable, in this case, *time*, is expressed as a polynomial function of geographic coordinates (X_i, Y_i) of individual case-points i. e., *time* = *f* (*X*, *Y*), a model known as a polynomial regression (*6*). The order of the polynomial chosen as the best

fit-model or the best polynomial equation will determine the shape of the curve or surface. Here, we used a third-order polynomial. The variable *time* (in days) was created using the symptoms onset date from the index case (IC) as the baseline date across the 810 case localities, this is, *time* (X_i, Y_i). Thus, *time* is considered as the number of days elapsed between the appearance of a case in a specific locality *Zi* and the IC. Results of the TSA were used to generate a contour map or smoothed surface, with each contour line representing a specific predicted time-period in this urban landscape setting since the initial invasion of the virus. Finally, we proceeded to estimate the local rate and direction of the spread of infection as the directional derivative at each case using the TSA fitted model to obtain local vectors that depicted the direction and speed (inverse of the slope along the direction of the movement) of infection propagation from each locality in *X* and *Y* directions. To this end, we calculated partial differential equations of *time* with respect to the *X*- and *Y*-coordinates (**∂***T*IME/**∂***X* and **∂**TIME/**∂***Y*) to obtain local vectors that depicted the direction and speed (inverse of the slope along the direction of the movement) of infection propagation from each locality in *X* and *Y* direction. The resultant vector for each case will represent, in turn, the overall velocity (in m/day) and direction of disease spread in each point. The set of vectors were assembled in a vector field and overlapped over the fitted surface to visualize the pattern of local spread of the virus along the urban landscape. TSA has been previously used to study pathogen dispersal processes in space and time (*7*). Further details of this methodology can be found in Moore (*8*) and Adjemian *et al*., (*9*). All the analyses were carried out in R software (The R-Development Core Team). Maps of time contours and vectors were generated in the ArcGIS software (v.10.3, ESRI Corporation, Redlands, CA), while general maps were constructed using Quantum GIS 2.14.3 Essen (GNU—General Public License).

1.4. KRIGING INTERPOLATION

Kriging is a local interpolation method based on a set of linear regressions that determine the best combination of weights to interpolate the data points by minimizing the variance as derived from the spatial covariance in the data (*10*). The weights are based on the spatial parameters of a theoretical variogram model such that sampling locations within the spatial range (close distances) of influence has more weight on the predicted value than the distant locations. Although kriging and trend surface analysis share some features (i.e., to describe the general spatial trend), the local interpolation performed by kriging shows an enhanced picture of the local spatial pattern given that the kriged values are very close to the observed ones. Kriging analyses (and resulting surface maps) were carried out in the Geostatistics tool from the ArcGIS software (v.10.3, ESRI Corporation).

1.5. SPATIOTEMPORAL ANALYSIS

Even though CHIKV was introduced into a naïve population, i.e., the individuals had a similar immunological likelihood of becoming infected, we wanted to assess the hypothesis of heterogeneity during disease transmission. In this sense we aimed to find whether aggregation of cases was present during the CHIK epidemic and if the likelihood of being infected could have varied depending on space and time distances. Thus, to identify general space-time aggregation (clusters) of CHIK transmission during the whole epidemic (28 weeks) we performed the Knox analysis (*11*) and the incremental Knox test (IKT) proposed by Aldstadt in 2007 (*12*) to identify linked transmission events.

1.5.1. KNOX TEST

This method measures potential space–time interactions by analyzing pairs of cases that belong to a particular space (distance) and time (days) window. This intuitive method provided simplicity and promptness (*13*). Yet, the Knox test requires prior selection of a "critical" time and distance to classify whether the pairs are close in space, or in time, or both. The test statistic, *X*, is the number of pairs of cases that are close in both space and time, and its calculated as

$$X(s,t) = \sum_{i=1}^{N} \sum_{j=1}^{i=1} a_{ij}^{s}\, a_{ij}^{t}$$

where *s* and *t* being the selected spatial and temporal distances, *N* is the number of cases, and the pair of cases are represented by *i* and *j*. The exact p value is obtained by the Monte Carlo procedure.

To select the "critical" value of space and time for our analysis, we performed a series of repetitions of the Knox method varying the time windows from 1 to 4 weeks (30 days in total) and the space window ranging from 25 to 200 m. Such analyses were made using the software ClusterSeer 2.0 (Terraseer, Ann Arbor, MI), which provides the graphical output of the space–time interactions (10.000 Monte Carlo iterations). The relative risk (RR) of each space and time window was calculated according to Tran *et al*. (*14*); where the RR is considered to be the ratio between the observed number of pairs of cases found at the space-distance s (in meters) and the time-distance t (in weeks) and the number of expected pairs of cases found at these same distances.

1.5.2. INCREMENTAL KNOX TEST

The incremental Knox test (IKT) is similar to other tests of the general hypothesis of space–time dependence (cases close to one another are much more likely to interact than cases far apart). However, this technique tests the interaction at specific time intervals rather than the more general space–time interaction hypothesis. The IKT examines consecutive links in the chain of transmission by identifying significant clusters in determined space and time intervals. The test assumes that cases that are nearer together than would be expected in the absence of an infectious process belong to one similar linked event of transmission (*12*).

Therefore, the IKT was used to understand in which time interval the clusters of cases of CHIK belonging to the same chain of transmission occurred helping to understand the linked transmission processes occurring in certain temporal span. The interval Knox statistic is formulated as

$$IK(s,t) = \sum_{i=1}^{N} \sum_{j=1}^{i=1} a_{ij}^{s}\, b_{ij}^{t}$$

Were *s* and *t* are the selected spatial and temporal distances, *N* is the number of cases, and the pair of cases are represented by *i* and *j*. When the cases *i* and *j* are time interval (*t*) apart . The Monte Carlo procedure with 10.000 iterations was used to construct reference distribution for *IK* (Z values) and the test results are also reported as the epidemiologic notion of excess of risk (details of this methodology can be found in [*12*]). over the time intervals from 1 to 31 days, and

space distances from 25 to 500 m (selected distances in metes: 25, 50, 75, 100, 125, 150, 175, 200, 300, 400, 500).

2. RESULTS

From surveillance data collected during the months following the introduction of CHIKV, the dynamics and timing of the 810 chikungunya reported cases were studied. Appendix Figure 1 depicts the distribution of cases and cumulative cases along the 28 weeks of the chikungunya epidemic. Since the detection of the index case (IC) in June of 2014, the north-central region of Venezuela experienced a continuous reporting of chikungunya cases. During the first 9 weeks (epidemiologic week [EW] 21-EW 29), a low number of cases were reported. After EW 30 cases increased rapidly with the exponential growth of the epidemic being observed between EW 30 and EW 33. The cumulative cases during the EW 22–49 followed a logistic growth (Appendix Figure 1: $R = 0.99$, n = 810, $p < 0.05$) reaching the plateau at EW 44 (787 cases). The total growth rate estimated from the logistic fitted curve was 0.53 cases per EW.

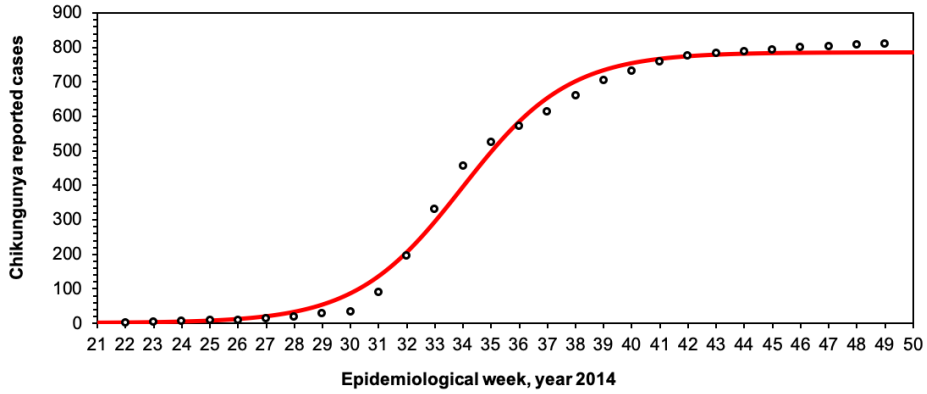

Appendix Figure 1. Logistic fitted model for reported chikungunya cases during the epidemic of 2014 in Carabobo State, Venezuela. Chikungunya cases are depicted by open black dots, red line depicts the fitted curve (logistic model).

2.1. REPRODUCTIVE NUMBER (R_0) AND EFFECTIVE REPRODUCTIVE NUMBER (RT)

To better understand the CHIK transmission dynamic, the basic reproductive number (R_0) was calculated during the exponential growth of the epidemic, that is during (EW 21–EW 33). During these first 12 weeks, the maximum value of R_0 reached was equal to 3.7 secondary chikungunya cases per primary case. Furthermore, we estimated the effective reproductive number (Rt) with a reporting interval of 1 week, to assess changes of R_0 through time. The curve of Rt values fluctuates in time as shown in Appendix Figure 2, where the maximum value of Rt obtained was 4.7 (95% CI 2.4–7.1) occurring during the EW 31 (Appendix Figure 2). Both measures are similar in principle, and estimate the transmission dynamic of the disease whether is at the initial phase of the epidemic (R_0) or as an estimate for the whole epidemic (Rt). The usefulness of Rt is the possibility to estimate its uncertainty (confidence interval) throughout the epidemic curve. This could be relevant and applicable to other diseases as well. Due to the intrinsic variability of the Rt series, the examination of its credible intervals is essential to identify periods of sustained transmission (*5*).

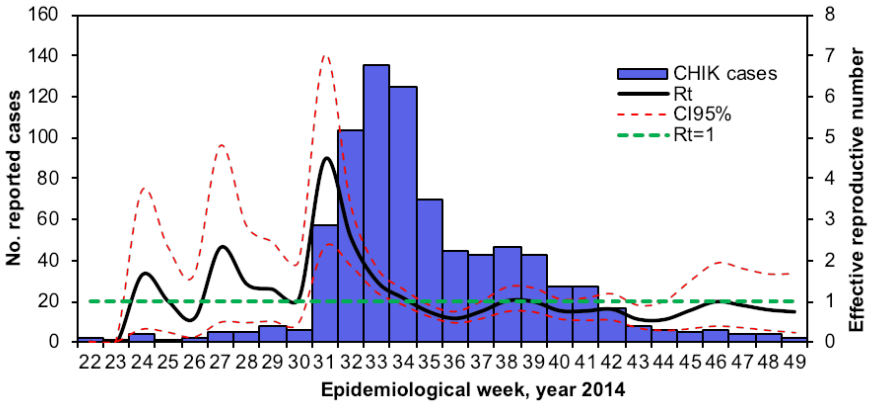

Appendix Figure 2. Reproduction number of chikungunya fever in Carabobo State, Venezuela, during 2014. Blue bars show the epidemic curve; the cases are shown in a weekly interval. Solid black line corresponds to the estimated Rt for the epidemic, dashed red line depicts the 95% CI, whereas green dashed line depicts the threshold Rt = 1.

2.2. KRIGING INTERPOLATION

We performed an ordinary kriging using 3 anisotropic variogram models. The models were compared by cross-validation and evaluated in terms of their overall robustness: optimality and validity of the model to fit the observed data (Appendix Table 1, Appendix Figure 3). Overall, all the models underestimated the variability in their predictions as is shown by: i) negative values of the mean standardized errors (MSE), ii) average standard error (ASE) values lower than the root-mean-squared prediction error (RMSE) values, and iii) standardized root-mean-squared prediction error (RMSSE) values >1 (Appendix Table 1). This can be due to too few sampled locations within the spatial range of the study area. However, our best selected model (Gaussian) was the one that had the MSE nearest to 0, the smallest RMSE, the ASE nearest to the RMSE, and a RMSSE nearest to 1 (15).

Table S1. Average velocities of chikungunya virus spread across Carabobo State, Venezuela, 2014

Model	Nugget (C_0) Range (a) Partial Sill (C_1)	MSE	RMSE	ASE	RMSSE
Gaussian	8.88				
	30.89	-0.014	17.35	14.29	1.18
	188.42				
Spherical	0.05				
	48.84	-0.015	17.45	11.04	1.53
	117.51				
Exponential	2.06				
	984.85	-0.016	18.13	15.07	1.40
	388.71				

*ASE, average standard error; MSE, mean standardized error; RMSE, root-mean-square error; RMSSE, root-mean-square standardized error.

The model was adjusted for the directional spatial trend of our data (anisotropy) in the semivariogram (10). Maps showing the kriging standard errors of the Gaussian model and of the other 2 models (for comparison) are presented in Appendix Figure 3. Darker colors in the error map (Appendix Figure 3) show larger kriging standard errors. Overall, the model failed to predict in areas out of the main spatial range of the data (where there are fewer and scarcer case locations) and showed a better prediction toward the south-west and eastern zones of the study area where a larger number of locations are presented. Indeed, this analysis identified a faster propagation of the epidemiologic wave at the south-west and eastern areas where the model showed its better fit (Appendix Figure 3, panel a), and a slower movement to the north-east and south-center areas.

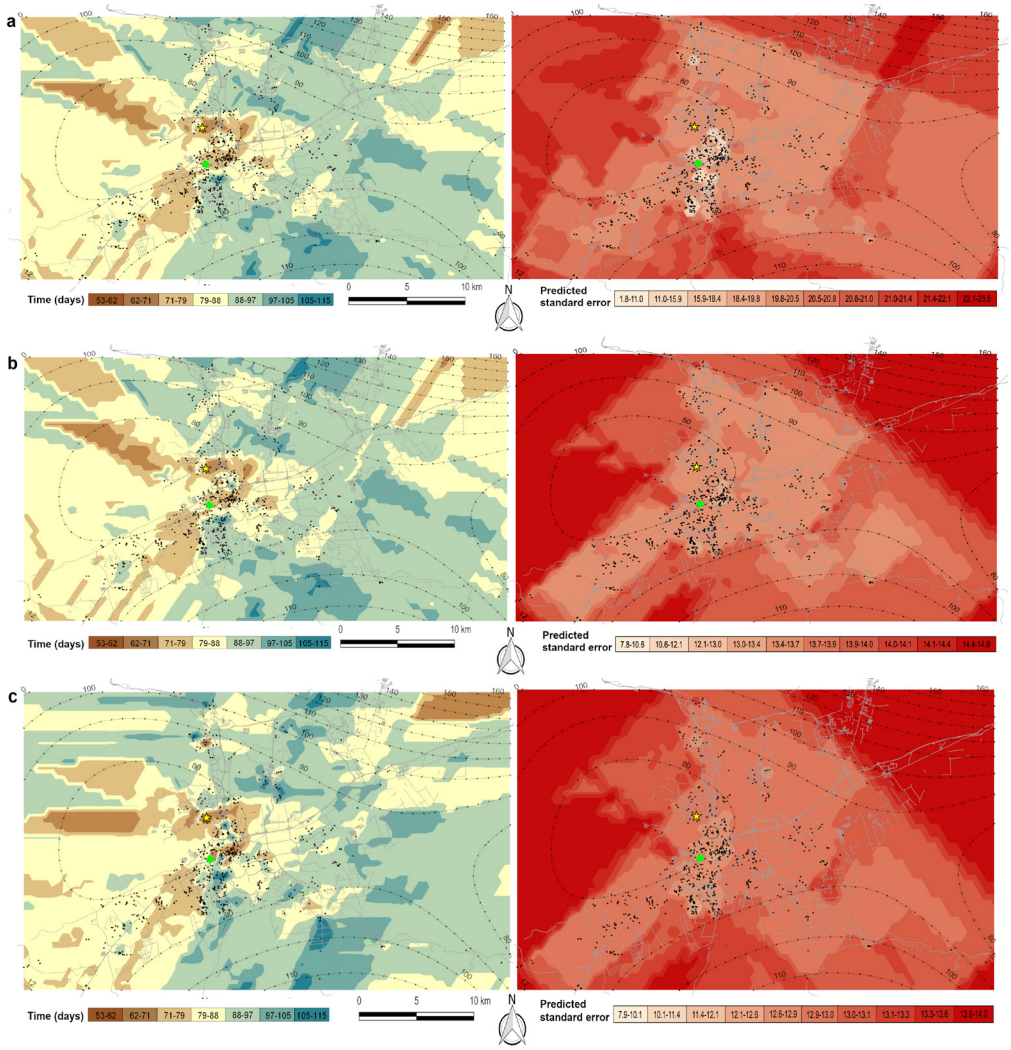

Appendix Figure 3. Spatial prediction map for the ordinary kriging interpolation of number of days elapsed between the appearance of a case in a specific locality and the IC obtained using the Gaussian (A), spherical (B), and exponential (C) models. Surface maps showing the kriging standard errors for each model in the right side of each map.

2.3. KNOX TEST

The results obtained after the analysis with different critical values of s and t showed that the core clusters (main clusters) found at week 1 (25–200 m) are the same than those (core clusters) found at week 2, 3, and 4 (25–200 m), therefore, we have selected to show on Appendix Figure 4 the graphical output of the critical values of t with a fixed space window of 100 m. However, the size of the core clusters is susceptible to the change of the space and time windows, making the clusters bigger or smaller in terms of number of links (Appendix Table 1), i.e., from 164 space-time links (1W,100 m) to 220 space-time links (3W,100 m).

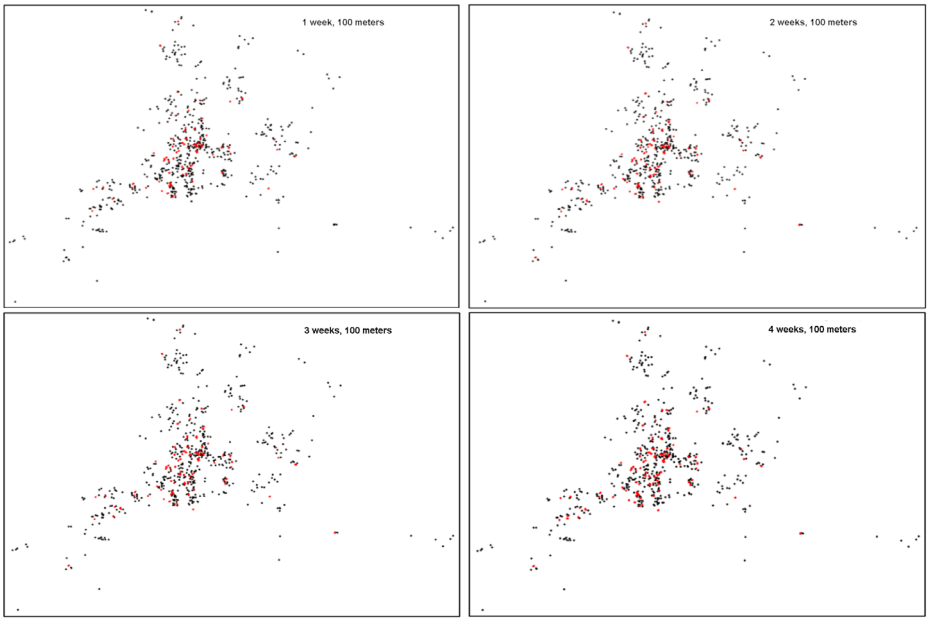

Appendix Figure 4. Space–time output varying the time window from 1 to 4 weeks. In red, the space-time clusters. Distance window was set at 100 m.

Regarding the RR at different space and time windows (Appendix Table 1), the highest RR were found at the space–time window of 1 week and 25–200 m (RR = between 3 and 2), but also showing RR >1.5 up to week 3 at the same space windows, while from week 4, values showed RR <1.5 (Appendix Figure 5). These results provided useful information that allowed to observe the extent of the interaction of s and t values that shows the highest RR. Hence, RR values that show an important strength of association are present up to week 3 (21 days) within a distance that varies between 25 and 150 m. This agrees with previous results obtained by Vincenti-Gonzalez et al. (16) for Venezuela, where the significant hot spots of high dengue seroprevalence values were found between 25–100 m, suggesting a focal transmission.

Even though the RR in week 3 decreased along the different distances (average 32 ± 7%) when compared to the RR of week 1, the RR remained higher than one (RR>1) in week 3. Given the fact that the Knox test results showed the same core clusters along the different t windows and the RR remained epidemiologically relevant after 3 weeks (general clustering of symptoms onset date, and RR>1), we used the window of 3 weeks with a distance window of 100 m to show the

global clusters of transmission (Appendix Figure 6). We decided to choose these distance and time variables based on biologic and ecologic knowledge as explained in the manuscript and in agreement with other authors (*17,18*). Where 100 m is the distance referred by most as the average flight range radius of *Aedes* spp. and a time window of 3 weeks gives enough time span for most transmission events to occur (*19-21*).

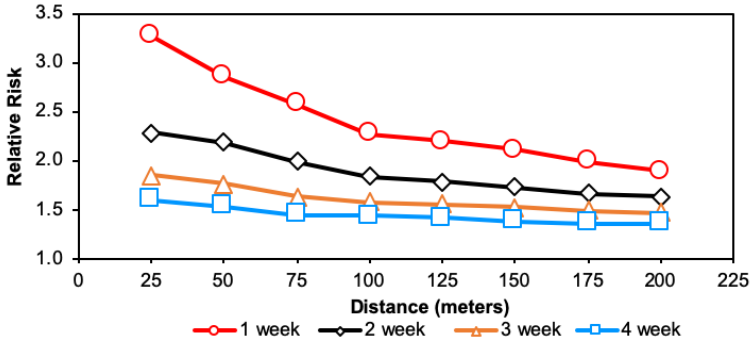

Appendix Figure 5. Relative risk from the Knox test with alternative definitions of spatial and temporal proximity.

2.3.1. GENERAL CLUSTERS OF TRANSMISSION EVENTS DURING THE EPIDEMIC WAVE OF CHIKUNGUNYA

Our results (Appendix Table 3) show that the average cluster duration since the symptoms onset of the first case to the symptoms onset of the last case within the clusters is 12.5 days ranging from 1–67 days. The choosing of 100 m does not preclude the finding of larger distances between cases within a cluster as the range of distances found was between 8–216 m. We expect that within clusters >1 chain of transmission will occur each with a duration of ~1 week or less.

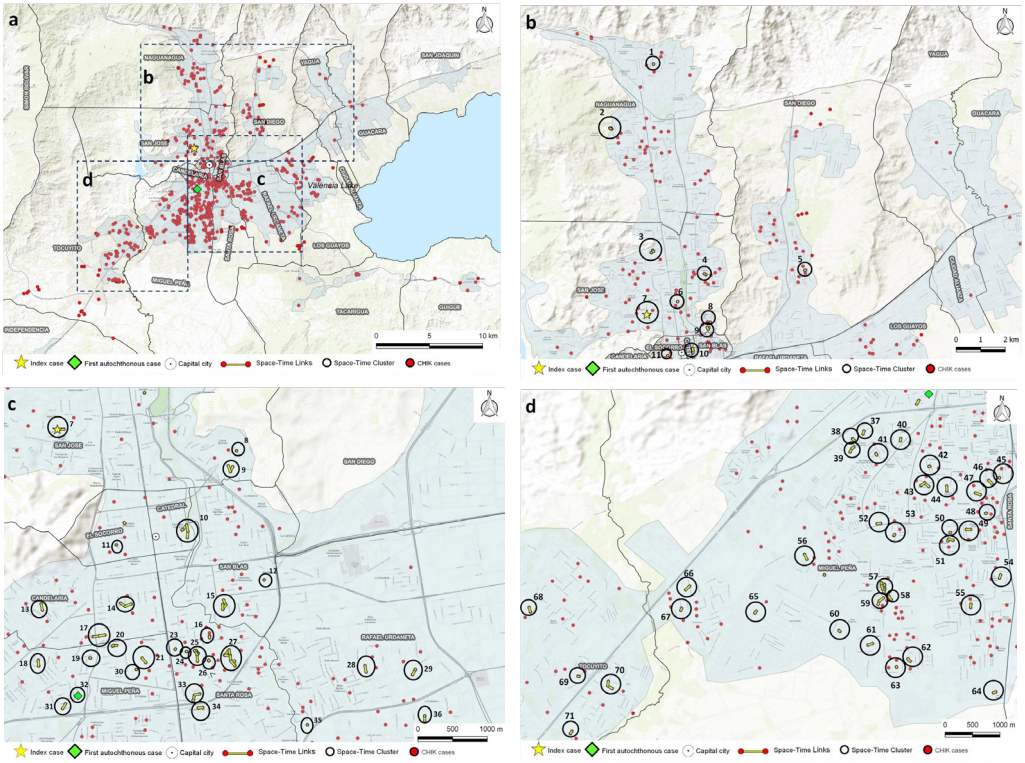

Appendix Figure 6. A) Geographic distribution of chikungunya reported cases in Carabobo state, Venezuela. a) Red dots denote case location, black dashed lines (b, c, d) are the different panels division (arbitrary) within Carabobo state selected to show in detail (zoom in) the general clusters of transmission. B) Geographic distribution and significant space–time clustering of chikungunya reported cases. Zoom in of the different cluster of transmission detected (including the IC), red dots denote case location, black circles identify a significant space–time cluster and yellow lines shows the interaction between cases (time–space link). The analysis was performed using 100 m as clustering distance and 3 weeks as time window. Significance level for local clustering detection was of 0.05. C) Geographical distribution and significant space-time clustering of chikungunya reported cases. Zoom in of the different cluster of transmission detected (including IC and AC), red dots denote case location, black circles identify a significant space-time cluster and yellow lines shows the interaction between cases (time-space link). The analysis was performed using 100 m as clustering distance and 3 weeks as time window. Significance level for local clustering detection was of 0.05. D) Geographic distribution and significant space–time clustering of chikungunya reported cases. Zoom in of the different cluster of transmission detected (including IC and AC), red dots denote case location, black circles identify a significant space–time cluster and yellow lines shows the interaction between cases (time–space link). The analysis was performed using 100 m as clustering distance and 3 weeks as time window. Significance level for local clustering detection was of 0.05.

2.4. Incremental Knox Test

The IKT was the second method used to assess the uncertainty of the cluster analysis. The previous was made employing an exploratory mode where the p-values (Appendix Figure 7) and the RR (Appendix Figure 8) were examined for a range of values of s and t. The results of the IKT analysis proved to be useful to identify linked transmission events, and showed that the temporal intervals with the strongest spatial clustering (belonging to the same chain of transmission) and RR occurs between 1–7 days suggesting multiple vector feeding within a gonotrophic cycle (22), with less strong clustering around 12–14 days. High RR results within 1 week are consistent for all tested distances, but values of RR >5 were found to be in distances between 25 and 150 m (Appendix Figures 7, 8), favoring our previous selection of a space-time window of 100 m.

Time (days) \ Distance (meters)	25	50	75	100	125	150	175	200	300	400	500
1	0.00	0.00	0.00	0.00	0.00	0.00	0.00	0.00	0.00	0.00	0.00
2	0.00	0.00	0.00	0.00	0.00	0.00	0.00	0.00	0.00	0.00	0.00
3	0.00	0.00	0.00	0.00	0.00	0.00	0.00	0.00	0.00	0.00	0.00
4	0.00	0.00	0.00	0.00	0.00	0.00	0.00	0.00	0.00	0.00	0.00
5	0.12	0.13	0.00	0.02	0.01	0.02	0.00	0.00	0.00	0.00	0.00
6	0.76	0.83	0.07	0.02	0.00	0.00	0.00	0.00	0.00	0.00	0.00
7	0.87	0.90	0.22	0.04	0.03	0.02	0.00	0.00	0.00	0.00	0.00
8	0.59	0.81	0.15	0.03	0.00	0.00	0.00	0.00	0.00	0.00	0.00
9	0.86	0.95	0.48	0.52	0.10	0.02	0.12	0.08	0.04	0.05	0.01
10	0.53	0.76	0.67	0.86	0.23	0.19	0.54	0.46	0.11	0.04	0.01
11	0.81	0.73	0.62	0.76	0.68	0.63	0.88	0.64	0.37	0.06	0.03
12	0.91	0.83	0.80	0.86	0.88	0.82	0.74	0.28	0.03	0.00	0.00
13	0.79	0.26	0.15	0.24	0.16	0.20	0.08	0.02	0.04	0.00	0.00
14	0.76	0.22	0.50	0.34	0.27	0.36	0.12	0.01	0.04	0.00	0.01
15	0.74	0.11	0.22	0.14	0.11	0.22	0.26	0.20	0.33	0.04	0.10
16	1.00	0.95	0.99	0.92	0.89	0.89	0.75	0.42	0.64	0.59	0.60
17	1.00	0.99	0.99	0.97	0.67	0.59	0.49	0.40	0.63	0.40	0.43
18	1.00	0.98	0.98	0.95	0.60	0.29	0.13	0.03	0.17	0.06	0.02
19	1.00	0.98	0.98	0.83	0.53	0.44	0.38	0.32	0.15	0.01	0.00
20	1.00	1.00	0.99	0.98	0.96	0.78	0.68	0.64	0.22	0.03	0.01
21	1.00	1.00	1.00	0.91	0.96	0.94	0.93	0.94	0.43	0.08	0.11
22	1.00	1.00	0.99	0.94	0.92	0.87	0.69	0.74	0.67	0.77	0.61
23	0.98	0.99	0.98	0.87	0.90	0.96	0.82	0.78	0.65	0.24	0.26
24	0.97	0.99	1.00	1.00	0.98	0.99	0.88	0.94	0.79	0.76	0.78
25	0.97	0.99	1.00	0.99	0.97	0.98	0.94	0.98	0.81	0.65	0.74
26	1.00	1.00	1.00	0.99	0.96	0.98	0.95	0.98	0.92	0.97	0.87
27	1.00	1.00	1.00	0.96	0.98	0.99	0.98	1.00	1.00	0.96	0.82
28	0.96	0.99	0.99	0.98	0.99	1.00	0.99	0.96	0.92	0.61	0.43
29	0.96	0.98	0.96	0.90	0.99	0.99	1.00	0.95	0.54	0.30	0.61
30	0.96	0.92	0.35	0.36	0.65	0.61	0.83	0.52	0.10	0.28	0.65
31	1.00	0.98	0.32	0.33	0.62	0.66	0.86	0.86	0.38	0.80	0.91

Appendix Figure 7. Significant values of the exploratory IKT analysis. In red the significant (p value <0.05) of space–time interactions within the specific space–time intervals.

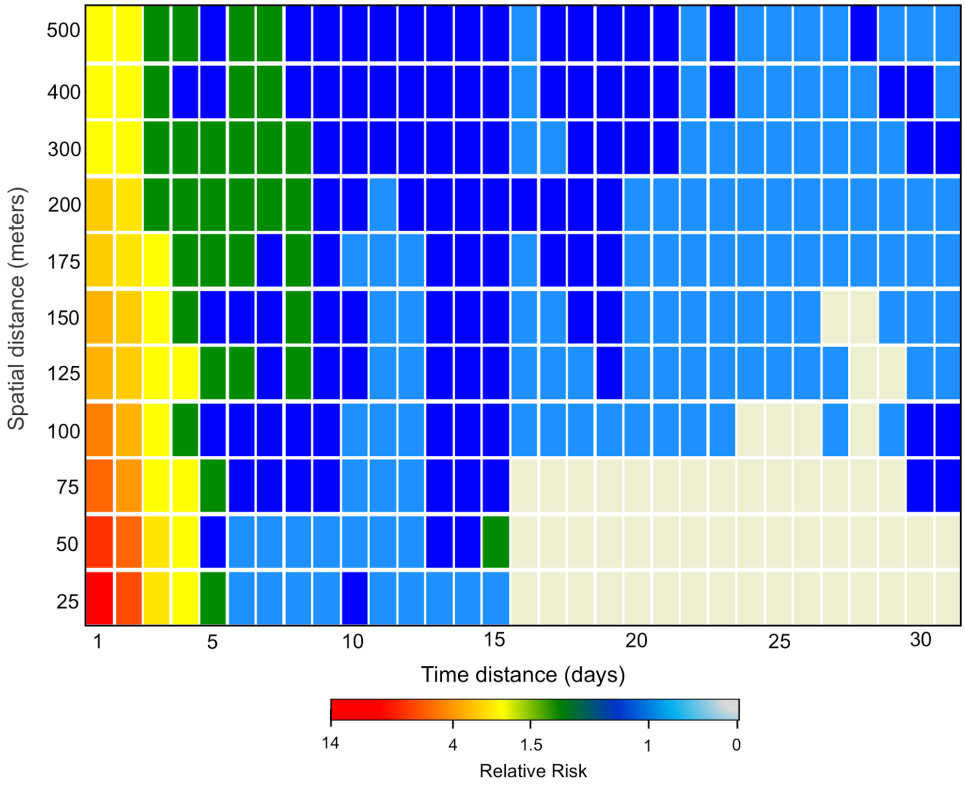

Appendix Figure 8. Values of relative risk for the exploratory IKT analysis. The colors in the heatmap depict the range of values of RR (refer to the legend) within the specific space–time intervals.

Appendix Table 2. Knox test with alternative definitions of spatial and temporal proximity*

TIME, WK	DISTANCE, M	EXPECTED	OBSERVED	RR
1	25	22	72	3.27
	50	28	81	2.86
	75	45	117	2.57
	100	72	164	2.27
	125	97	213	2.20
	150	122	258	2.11
	175	159	316	1.99
	200	199	376	1.89
2	25	34	77	2.28
	50	44	95	2.18
	75	70	138	1.98
	100	110	202	1.83
	125	148	264	1.78
	150	187	322	1.72
	175	243	404	1.66
	200	304	497	1.63
3	25	43	79	1.85
	50	55	97	1.76
	75	88	144	1.63
	100	140	220	1.57
	125	188	293	1.56
	150	237	360	1.52
	175	308	457	1.48
	200	386	566	1.47
4	25	50	80	1.59
	50	65	99	1.53
	75	104	150	1.45
	100	164	236	1.44
	125	221	313	1.42
	150	279	383	1.37
	175	362	493	1.36
	200	453	617	1.36

*MONTE CARLO SIMULATIONS PERFORMED IN EACH ANALYSIS:10.000.

Appendix Table 3. Description of the space–time cluster identified for the chikungunya epidemic in the north-central region of Venezuela.

Cluster ID	No. cases	Day occurrence, first–last case	Cluster duration, d	Average distance from IC, m	Range of distance from IC, m	Velocity average, m/day	Velocity range, m/day
1	2	95–105	11	10132.0	10128–10136	102.0	97–107
2	4	77–105	29	7659.8	7636–7686	86.8	73–100
3	4	72–85	14	2556.0	2818–2613	32.3	30–36
4	3	72–94	23	2872.0	2857–2898	33.7	30–40
5	2	121–126	6	6685.5	6661–6710	54.0	53–55
7	3	0–25	26	31.7	0–95	1.3	0–4
8	2	125–135	11	2598.5	2598–2599	20.0	19–21
9	3	64–95	78	2553.7	2515–2585	33.3	27–34
10	5	71–99	29	2344.0	2299–2429	29.6	24–33
11	2	73–73	1	1857.0	1856–1858	25.0	25.0
12	2	61–61	1	3673.5	3673–3674	60.0	60.0
13	2	73–80	8	2550.0	2506–2594	33.4	32–34
14	4	79–107	29	2680.3	2647–2714	29.0	25–34
15	5	72–108	37	3463.0	3418–3508	43.4	32–51
16	3	43–57	15	3687.0	3680–3700	75.3	65–86
17	3	3–31	33	3015.3	3011–3020	45.3	39–50
18	2	91–99	9	3354.5	3315–3394	35.0	33–37
19	2	47–60	14	3305.0	3304–3306	62.5	55–70
20	3	63–78	16	3198.3	3192–3205	46.0	41–51
21	2	61–82	22	3531.5	3491–3571	50.5	44–57
23	2	66–66	1	3573.0	3571–3575	54.0	54.0
24	2	65–65	1	3684.0	3683–3685	57.0	57.0
25	9	59–72	14	3786.2	3734–3882	57.8	54–64
26	3	75–88	14	3967.0	3957–3967	53.0	45–53
27	12	69–77	9	4092.8	4008–4241	57.8	54–59
28	2	66–68	3	5608.5	5643–5574	83.5	83–84
29	3	0–66	67	6799.0	6194–6204	97.0	94–103
30	2	67–68	2	3617.0	3616–3618	53.5	53–54
31	2	74–80	7	3970.0	3929–3997	51.5	49–54
32	2	16–19	4	3822.0	3820–3824	220.0	201–239
33	5	65–82	18	4311.7	4282–4344	59.8	53–66
34	2	67–72	6	4483.0	4471–4495	64.5	62–67
35	2	88–94	7	5555.0	5554–5556	61.0	59–63

36	3	89–109	21	6709.7	6694–6739	67.7	61–76
37	2	72–76	5	4601.0	4571–4631	62.0	61–63
38	3	86–88	3	4760.3	4752–4775	54.3	54–55
39	3	68–86	19	4940.3	4894–4998	62.3	57–72
40	2	76–76	1	4645.5	4623–4668	61.0	61.0
41	2	61–64	4	4938.0	4938–4964	77.0	77–81
42	2	50–63	14	5138.0	5138.0	103.0	82–103
44	2	103–107	5	5561.5	5518–5605	53.0	52–54
45	2	116–117	2	5564.5	5562–5567	48.0	48.0
46	2	119–121	3	5596.0	5536–5556	47.0	47.0
47	2	108–115	8	5750.5	5727–5774	51.5	50–53
48	2	92–101	10	6126.5	6126–6127	64.0	61–67
49	2	80–80	1	6356.0	6349–6363	79.5	79–80
50	2	76–76	1	6368.5	6368–6369	84.0	84.0
51	3	103–132	30	6501.6	6512–6479	56.0	49–63
52	2	85–85	1	6796.5	6191–6202	73.0	73.0
53	2	75–111	37	6382.5	6373–6392	71.0	57–85
54	2	99–103	5	7305.5	7279–7332	72.5	71–74
55	2	92–103	12	7734.5	7704–7765	79.5	84–75
56	2	60–74	15	7046.0	7011–7081	106.5	96–117
57	6	60–77	18	7341.8	7262–7428	108.3	96–122
58	2	81–83	3	7526.5	7495–7558	92.0	91–93
59	3	63–72	10	7598.6	7535–7661	112.3	106–120
60	2	76–76	1	8228.5	8221–8626	108.0	86–97
61	2	72–76	5	8396.0	8381–8411	113.5	111–116
62	2	89–100	12	8647.5	8626–8669	91.5	86–97
63	2	86–86	1	8778.5	8774–8783	102.0	102.0
64	2	102–115	14	9355.0	9349–9361	86.5	81–92
65	2	76–76	1	8228.5	8221–8236	108.0	108.0
66	2	75–80	6	8406.0	8359–8453	108.5	106–111
67	2	80–80	1	8804.0	8783–8825	110.0	110.0
68	2	79–79	1	10419.5	10397–10442	132.0	132.0
69	2	83–84	2	10822.0	10819–10825	129.5	129–130
70	3	70–85	16	10653.7	10603–10679	135.7	125–153
71	2	142–163	22	11749.5	11726–11776	77.5	72–83
72	5	69–99	31	7611.0	7599–7622	103.4	77–110
73	2	59–81	23	7943.0	7920–7966	116.5	98–135
74	3	70–92	23	12291.7	12224–12341	153.7	134–175
75	2	134–136	3	9903.5	9903–9904	73.5	73–74

76	2	65–79	15	7636.5	7630–7643	107.5	97–118
77	2	78–78	1	1651.5	1644–1659	21.0	21.0
78	3	129–133	5	5477.0	5477.0	41.7	42.0

Results shown here describes the general clusters of transmission found by Knox analysis with the critical values set at 100mts as clustering distance and 3 weeks as time window. Monte Carlo performed, 10.000

Appendix Table 4. Linear distance between cases within the major spatiotemporal clusters

Cluster ID	No. cases	Average distance, m	Stddev, m	Maximum, m	Minimum, m
Cluster 10	5	77.0	47.2	130.7	16.2
Cluster 14	4	130.7	27.3	150.4	92.1
Cluster 15	5	63.6	23.7	85.4	30.0
Cluster 02	4	38.2	16.4	54.6	21.9
Cluster 25	9	61.9	26.5	66.4	26.2
Cluster 27	12	81.6	19.2	216.0	8.0
Cluster 33	5	78.6	1.1	79.8	77.6
Cluster 33	4	85.6	26.5	105.0	55.4
Cluster 57	6	77.8	28.9	124.0	54.1
Cluster 72	5	56.7	39.1	93.7	10.3
Average	6	75.2	25.6	110.6	39.2

4. REFERENCES

1. Wallinga J, Lipsitch M. How generation intervals shape the relationship between growth rates and reproductive numbers. Proc Biol Sci. 2007;274:599–604.
2. Boëlle P-Y, Thomas G, Vergu E, Renault P, Valleron A-J, Flahault A. Investigating transmission in a two-wave epidemic of chikungunya fever, Réunion Island. Vector Borne Zoonotic Dis. 2008;8:207–17. http://dx.doi.org/10.1089/vbz.2006.0620
3. Boëlle, P-Y & Obadia, T. 'R0': Estimation of R0 and Real-Time Reproduction Number from Epidemics. R package version 1.2-6. 2015. [20 Dec 2017]
4. Nishiura H, Chowell G, Heesterbeek H, Wallinga J. The ideal reporting interval for an epidemic to objectively interpret the epidemiological time course. J R Soc Interface. 2010;7:297–307.
5. Coelho FC, Carvalho LM. Estimating the attack ratio of dengue epidemics under time-varying force of infection using aggregated notification data. Scientific Reports. 2015;5:18455 doi:10.1038/srep18455
6. Legendre P, Legendre L. Trend surface analysis. Numerical ecology. Netherlands: Elsevier Science; 1998. p. 739–46.
7. Pioz M, Guis H, Calavas D, Durand B, Abrial D, Ducrot C. Estimating front-wave velocity of infectious diseases: a simple, efficient method applied to bluetongue. Vet Res (Faisalabad). 2011;42:60.
8. Moore DA. Spatial diffusion of raccoon rabies in Pennsylvania, USA. Prev Vet Med. 1999;40:19–32.
9. Adjemian JZ, Foley P, Gage KL, Foley JE. Initiation and spread of traveling waves of plague, Yersinia pestis, in the western United States. Am J Trop Med Hyg. 2007;76:365–75.
10. Dale M, Fortin M. Spatial analysis: a guide for ecologists. 2nd edition. United Kingdom: Cambridge University Press; 2014.
11. Knox EG. The detection of space-time interactions. Journal of the Royal Statistical Society. Series C, Applied Statistics. 1964;13(1):25–29.
12. Aldstadt J. An incremental Knox test for the determination of the serial interval between successive cases of an infectious disease. Stochastic Environmental Research and Risk Assessment. 2007;21:487–500.
13. Gear J. A test for detecting space-time clustering and a comparison with some existing methods [Doctoral dissertation]. Chapel Hill (NC): University of North Carolina; 2006:10–12. [20 Dec 2017]. Retrieved from:
14. Tran A, Deparis X, Dussart P, Morvan J, Rabarison P, Remy F, et al. Dengue spatial and temporal patterns, French Guiana, 2001. Emerg Infect Dis. 2004;10:615–21.
15. Johnston K, Hoef M, Krivoruchko K, Lucas N. Using ArcGIS geostatistical analyst. Redlands, CA: ESRI; 2001.
16. Vincenti-Gonzalez MF, Grillet ME, Velasco-Salas ZI, Lizarazo EF, Amarista MA, Sierra GM, et al. Spatial analysis of dengue seroprevalence and modeling of transmission risk factors in a dengue hyperendemic city of Venezuela. PLoS Negl Trop Dis. 2017;11:e0005317.
17. Vazquez-Prokopec GM, Kitron U, Montgomery B, Horne P, Ritchie SA. Quantifying the spatial dimension of dengue virus epidemic spread within a tropical urban environment. PLoS Negl Trop Dis. 2010;4:e920.
18. Vazquez-Prokopec GM, Montgomery BL, Horne P, Clennon JA, Ritchie SA. Combining contact tracing with targeted indoor residual spraying significantly reduces dengue transmission. Sci Adv. 2017;3:e1602024.
19. Harrington LC, Scott TW, Lerdthusnee K, Coleman RC, Costero A, Clark GG, et al. Dispersal of the dengue vector Aedes aegypti within and between rural communities. Am J Trop Med Hyg. 2005;72:209–20.
20. Rudolph KE, Lessler J, Moloney RM, Kmush B, Cummings DA. Incubation periods of mosquito-borne viral infections: a systematic review. Am J Trop Med Hyg. 2014;90:882–91.
21. Mbaika S, Lutomiah J, Chepkorir E, Mulwa F, Khayeka-Wandabwa C, Tigoi C, et al. Vector competence of Aedes aegypti in transmitting chikungunya virus: effects and implications of extrinsic incubation temperature on dissemination and infection rates. Virol J. 2016;13:114.
22. Aldstadt J, Yoon I-K, Tannitisupawong D, Jarman RG, Thomas SJ, Gibbons RV, Uppapong A, Iamsirithaworn S, Rothman AL, Scott TW, Endy T. Space-time analysis of hospitalised dengue patients in rural Thailand reveals important temporal intervals in the pattern of dengue virus transmission. Trop Med Int Health. 2012;17(9):1076-1085.